NASA TECHNICAL NOTE

NASA TN D-3197

NASA TN D-3197

RADIANT HEATING OF A SEEDED GAS IN A COAXIAL-FLOW GASEOUS REACTOR

by Charles C. Masser

Lewis Research Center

Cleveland, Ohio

NATIONAL AERONAUTICS AND SPACE ADMINISTRATION • WASHINGTON, D. C. • JANUARY 1966

NASA TN D-3197

RADIANT HEATING OF A SEEDED GAS IN A COAXIAL-FLOW GASEOUS REACTOR

By Charles C. Masser

Lewis Research Center
Cleveland, Ohio

NATIONAL AERONAUTICS AND SPACE ADMINISTRATION

For sale by the Clearinghouse for Federal Scientific and Technical Information
Springfield, Virginia 22151 – Price $1.00

RADIANT HEATING OF A SEEDED GAS IN A COAXIAL-FLOW GASEOUS REACTOR

by Charles C. Masser

Lewis Research Center

SUMMARY

A theoretical analysis was made to determine how effectively a seed material can heat hydrogen propellant in a coaxial-flow gas-core reactor. It was assumed that the seed material was spherical and that the heat-transfer mechanism was radiation from the hot gas core to the spherical particles and conduction from the particles to the surrounding hydrogen gas.

The following ranges of conditions were used: particle diameters from 0.05 to 1.00 micron; power outputs of the gas core from 3195 to 10 097 megawatts per foot of core length, which correspond to surface blackbody temperatures of 30 000° and 40 000° R, respectively; constant density and specific heat corresponding to 500 atmospheres and 5500° R for the hydrogen propellant; and three values of hydrogen gas thermal conductivity corresponding to temperatures of 2900°, 5500°, and 8000° R.

It is concluded that the difference between the particle and bulk gas temperatures can be kept under 500° R, and thus the propellant-seed mixture can be treated as a continuous gray gas. Several cases of high temperature differences of 1500° to 2000° R between the gas and the particles are computed, but these large temperature differences decrease quickly away from the heat flux source.

INTRODUCTION

In the coaxial-flow gas-core nuclear rocket concept (refs. 1 to 3) severe thermal radiation problems occur. All nuclear heat released from the core travels outward toward the reactor wall. The hydrogen propellant must absorb this heat in order to protect the rocket wall and reach the performance levels desired in the system; however, since hydrogen gas under 10 000° R is theoretically transparent to radiation, the difficulty of absorbing this radiation arises. One of the approaches used to solve this problem is the addition of small solid particles to the hydrogen. The seeded hydrogen will then absorb the radiated heat from the core.

In this system it is important to know how effectively the seeding particles can transfer heat from the hot gas core to the hydrogen propellant. Since the primary purpose is to heat the hydrogen gas, the difference between the par-

ticle temperature and the bulk gas temperature becomes an important quantity.

Some previous work in the area of radiant heating of gas containing particles has been reported. Theoretical investigations of the transmission properties of particles are given in references 4 and 5, whereas experimental data are reported in references 6 to 9. An analysis of temperature differences between a particle and a gas is reported in reference 10 for a particle in an infinite atmosphere. References 11 and 12 have extended this work to include a finite volume of gas associated with each particle.

It is the purpose of this report to extend the present knowledge to analyzing the radiant heating of a dispersion of spherical particles in a coaxial-flow reactor. In this analysis, particular interest is focused not only on the parameters that influence the temperature difference between the particles and the gas, but also on the way this temperature difference will vary with position in the gas-core nuclear rocket. Questions such as how does particle concentration affect the temperature difference and what part do heat flux and particle size play in the analysis must be answered. If this temperature difference is found to be insignificant, the hydrogen-propellant - particle mixture can be treated as a continuous gray gas of uniform absorptivity. If this temperature difference is significant, a correction factor must be used in calculating temperature profiles within the cavity of the nuclear rocket.

SYMBOLS

A	constant of integration
a	radius of particle, ft
B	constant of integration
c_p	specific heat, Btu/(lb)($^\circ$R)
k	thermal conductivity, Btu/(hr)(ft)($^\circ$R)
L	dimensionless constant, l/a
$\mathfrak{L}$	Laplace operator
l	one-half mean distance between particles, ft
N	particle concentration, particles/cu ft
Q	radiant heat flux, Btu/(hr)(sq ft)
q	heat, Btu
R	radial position in reactor, ft
r	radial position from particle center, ft

S Laplacian of t

T temperature, ^{o}R

t dimensionless time, $k_g\theta/(\rho c_p)_g a^2$

U dimensionless variable, $X(T - T_0)/T_0$

u Laplacian of U

V velocity, ft/sec

v Laplacian of $(T - T_0)/T_0$

X dimensionless variable, r/a

x path length, ft

Z axial distance in reactor, ft

α ratio of effective to actual cross-sectional area

θ time, hr

ρ density, lb/cu ft

σ effective cross-sectional area, sq ft

φ dimensionless constant, $(\rho c_p)_p/3(\rho c_p)_g$

Subscripts:

cl centerline

g gas

p particle

0 initial

ASSUMPTIONS

With the gas-core nuclear reactor (fig. 1) as a basis for this study, a model is first postulated that most clearly fits the existing situation (fig. 2). Various assumptions were used in forming the model so the associated differential equation could be solved. The assumptions were

(1) The seeding particles are to be spherical, and their diameter is not a

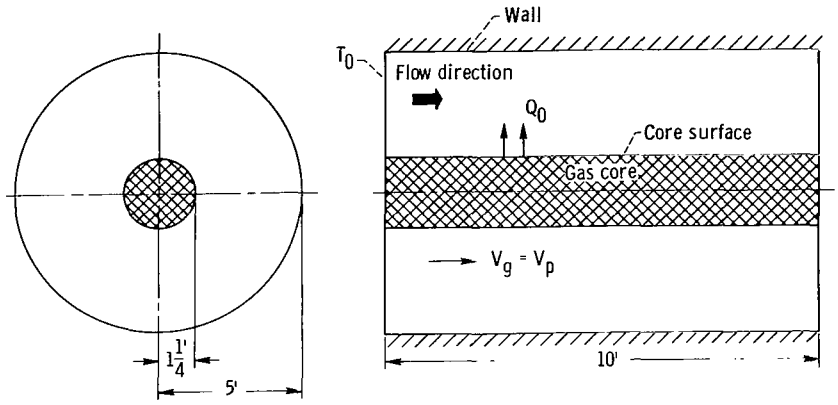

Figure 1. - Gas-core reactor model.

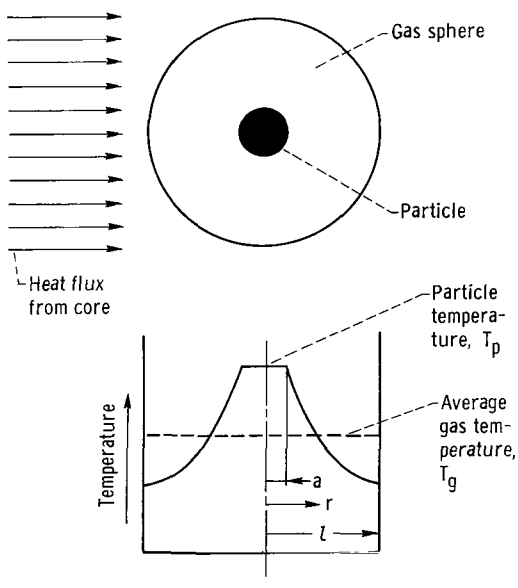

Figure 2. - Particle-gas model.

function of time.

(2) The temperature distribution within a particle is neglected.

(3) The particle absorption cross section is constant with temperature.

(4) The particles receive heat only by radiation, reject a percentage of this heat to the surrounding gas only by conduction, and retain the rest for increasing the internal energy of the particles.

(5) The energy radiated from the core surface travels outward in the radial direction only; reradiation from the particles, free convection, and axial and radial conduction are also assumed to be negligible.

(6) No relative velocity exists between the particles and the surrounding gas.

(7) The particles disappear (or are assumed to vaporize instantaneously) at a specified temperature of 8000° R, and the change in enthalpy for this process is zero.

(8) No temperature jump exists at the surface of the particles since the mean free path of hydrogen is small compared with the diameter of the particles.

Some explanation should be given for several of the assumptions used in this study. Since a spherical coordinate system was chosen for the particle-gas system (fig. 2), the use of spherical particles was made to facilitate the mathematics involved.

In order to use the assumption of no temperature gradients within the particle, the actual temperature distribution in the particle is solved for uniform internal absorption. For uniform internal absorption of a particle an energy balance on a spherical shell yields

$$\frac{k_p}{r^2}\frac{\partial}{\partial r}\left(r^2\frac{\partial T}{\partial r}\right) + \frac{3\alpha Q}{4a} = (\rho c_p)_p\frac{\partial T}{\partial \theta} \qquad r \leq a \tag{1}$$

where α is the ratio of radiation the particle absorbs to radiation the particle would absorb if it were a blackbody. The maximum temperature difference occurs at the steady-state condition:

$$\frac{k_p}{r^2}\frac{\partial}{\partial r}\left(r^2\frac{\partial T}{\partial r}\right) + \frac{3\alpha Q}{4a} = 0 \qquad r \leq a \tag{2}$$

A double integration yields

$$T = -\frac{\alpha Q r^2}{8ak_p}\Bigg|_{r=a}^{r=0} \tag{3}$$

which gives

$$T_{r=0} - T_{r=a} = \frac{\alpha Q a}{8k_p} \tag{4}$$

In the case of surface absorption the surface temperature of the particle is higher than that at the center. Therefore, a temperature gradient exists in the opposite direction from that in the case of uniform internal absorption. This temperature gradient approaches zero as time approaches infinity. The temperature gradient in a particle of nonuniform absorption can be assumed to be of the same order of magnitude as equation (4). The maximum temperature difference existing in a carbon particle will range from under 1 percent to 10 percent of the temperature difference that exists in the gas layer surrounding the particle. The low and high percentage levels correspond to high and low gas thermal conductivities, respectively.

From preliminary work on tungsten particles of 0.1-micron diameter (ref. 4), it appears that the absorption cross section of a particle is reasonably constant with temperature. With the low temperature differences found between the particles and the gas, relative to the particle temperature, free convection is neglected. Reradiation is also neglected since the temperature of the parti-

cle is at all times less than 30 percent of the core temperature.

It is also assumed that no relative velocity or eddy transfer exists between the particles and the surrounding gas. Data in reference 13, page 266, indicate this is true for a particle Reynolds number less than 2. From the diameter of the particle and the Stokes velocity in a gravity field, the particle Reynolds number for a 1-micron particle is essentially zero. In a true flow case where other forces besides gravity exist, such as turbulent forces, a relative velocity larger than the Stokes velocity may exist. The increased heat transfer from the particle due to this relative velocity would further reduce the temperature difference between the gas and the particles; therefore, the assumption of no relative velocity creates more severe temperature differences between the gas and the particles than would occur in a true flow case. End effects are ignored so that the energy can be assumed to radiate outward in the radial direction only.

The effects of particle vaporization are not included in this analysis; therefore, zero heat of vaporization was used to simplify the calculations. However, calculations were made in order to determine the maximum time for vaporization of the particles in question. This included the time that was required for the particle to attain its heat of vaporization plus the heat needed to raise the surrounding gas layer to the vaporization temperature of the particles. The times involved are 0.37×10^{-2} to 0.37×10^{-4} second for 1.0- and 0.1-micron-diameter particles, respectively, at a gas thermal conductivity of 0.852 Btu per foot per hour per $^{\circ}$R. The seeding rate was 0.314 pound per second, which leads to a ratio of gas sphere radius to particle radius of 94.8. These amounts of time are small compared with the residence time of 0.19 second for the particles in the reactor model itself.

When the mean free path of hydrogen approaches the size of the particles, the surface temperature of the particle is higher than the immediate gas layer surrounding the particle. At 500 atmospheres and 5000° R, the mean free path of hydrogen is 0.00273 micron, which is considerably less than any particle diameter used in the analysis; therefore, no temperature jump is experienced in this system.

Constant density and specific heat corresponding to 500 atmospheres and 5500° R were used for the hydrogen propellant. Three values of hydrogen gas thermal conductivity were used, which corresponded to temperatures of 2900°, 5500°, and 8000° R. The values of the hydrogen properties used were furnished by the author of reference 14.

ANALYSIS

An overall picture of the analysis will be presented before any single point is discussed in detail. When a sample calculation is examined, the first operation is computing the heat flux at the point in question. With this computed heat flux, the particle temperature is calculated from the solution of the differential equation controlling the model (fig. 2). At this point the total heat in the system and the heat contained in the particle are known as a func-

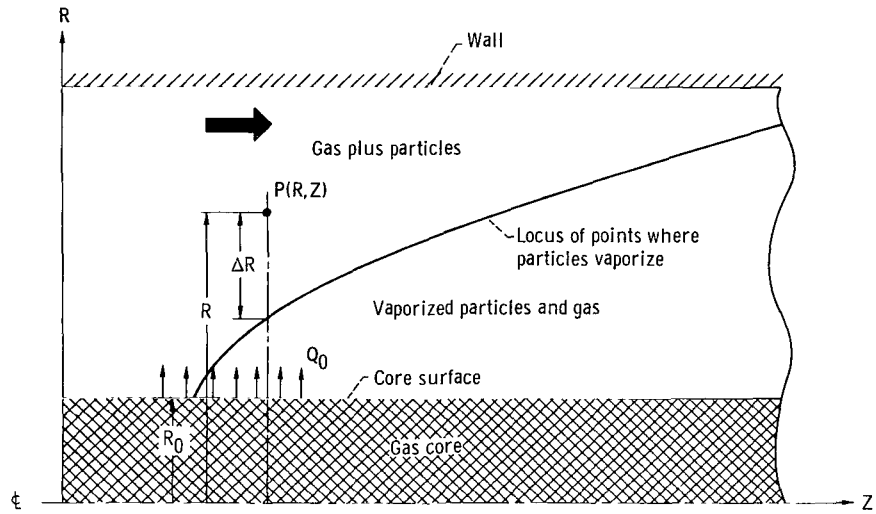

Figure 3. - Gas-core reactor cavity.

tion of time. A heat balance is then used to calculate the bulk gas temperature.

Since the heat flux varies throughout the R,Z-plane of the reactor model (fig. 3), a general expression for the spatial dependence of heat flux is needed. In figure 3 the overall picture is shown, where at point P(R,Z) it is desired to find the heat flux on a particle surface. From the Beer-Lambert law for radiation attenuation along a linear path of length x,

$$\frac{Q}{Q_0} = \exp\left(-\sigma \mathbb{N} x\right) \tag{5}$$

where σ is the absorption cross-sectional area, $\mathbb{N}$ is the particle concentration, and x is the path length. As a first approximation, the absorption cross-sectional area σ is simply the cross-sectional area of the particle multiplied by a dimensionless efficiency factor α; therefore σ can be expressed as

$$\sigma = \alpha \pi a^2 \tag{6}$$

where α is the efficiency factor, which can vary from 0 to 1 (ref. 8), and a is the particle radius. In this analysis, α was treated as an independent variable. In cylindrical coordinates, the path length x becomes ΔR, and in addition there is a geometric attenuation of heat flux that is proportional to the radius ratio. Therefore, for the present situation equation (1) can be written in the following form:

$$\frac{Q(R,Z)}{Q_0} = \frac{R_0}{R} \exp\left(-\alpha \mathbb{N} \pi a^2 \Delta R\right) \tag{7}$$

This equation for $Q(R,Z)$ is first solved for a particular location in the reactor model and is used in the equations that yield the particle and bulk gas temperatures.

In order to obtain the equation for the particle temperature as a function of time, an analysis of the gas-particle model (fig. 2) has to be made. An energy balance over a differential spherical shell of hydrogen gas surrounding the particle is performed. The resulting differential equation to solve is

$$\frac{k_g}{r^2}\frac{\partial}{\partial r}\left(r^2\frac{\partial T}{\partial r}\right) = (\rho c_p)_g\frac{\partial T}{\partial \theta} \qquad l > r > a \tag{8}$$

This is the standard heat conduction equation in spherical coordinates, and it can be found in reference 10, page 230.

The two boundary conditions are

$$\alpha Q(R,Z) = -4k_g\frac{\partial T}{\partial r} + \frac{4a}{3}(\rho c_p)_p\frac{\partial T}{\partial \theta} \qquad \text{at } r = a \tag{9}$$

$$\frac{\partial T}{\partial r} = 0 \qquad \text{at } r = l \tag{10}$$

The first boundary condition is an equality of heat fluxes at the surface of the particle. The term on the left side of the equation is the heat flux received by the particle. The first term on the right side of the equation is the heat flux into the gas, and the second term is the rate of increase of internal energy of the particle. The second boundary condition states that the temperature gradient is zero midway between particles. The initial condition is

$$T = T_0 \qquad \text{at } \theta = 0 \tag{11}$$

When Laplace transformations are used to solve the differential equation, there is obtained the particle temperature:

$$T_p - T_0 = \frac{\alpha a Q(R,Z)}{4k_g}\left\{1 - \exp\left[-\frac{3k_g\theta}{a^2(\rho c_p)_p}\right] + \frac{4\pi a N k_g\theta}{(\rho c_p)_g}\right\} \tag{12}$$

The derivation of equation (12) is given in appendix A.

From an energy balance on the gas-particle model (fig. 2), the difference between the particle temperature and the bulk gas temperature can be obtained:

$$T_p - T_g = \frac{\alpha a Q(R,Z)}{4k_g}\left\{1 - \exp\left[-\frac{3k_g\theta}{a^2(\rho c_p)_p}\right]\right\} \tag{13}$$

A detailed analysis showing the steps involved in obtaining equation (13) are shown in appendix B. Note at this point that the particle concentration N has no effect on the difference between the particle temperature and the bulk gas temperature. Equations (12) and (13) were obtained by assuming $L \gg 1$, and for the cases used in this study L is approximately 100.

Because of the large number of calculations, the equations were programed for the IBM 7094 computing machine so that a large number of cases could be solved in order to analyze the trends of several variables. The computer program used was made as general as possible for data input. The input parameters needed for the program are the following:

Initial temperature of particles and gas, $^{\circ}R$	3000
Weight flow of particles, lb/sec	0.314
Weight flow of gas, lb/sec	667.0
Gas core radius, ft	1.25
Reactor core radius, ft	5.00
Surface temperature range of core, $^{\circ}R$	30 000 to 40 000
Density of particles, lb/ft^3	100
Density of gas, lb/ft^3	0.249
Specific heat of particles, Btu/(lb)($^{\circ}R$)	0.876
Specific heat of gas, Btu/(lb)($^{\circ}R$)	4.95
Thermal conductivity range of gas, Btu/(ft)(hr)($^{\circ}R$)	0.387 to 2.884
Vaporization temperature of particles, $^{\circ}R$	8000
Diameter range of particles, μ	0.05 to 1.00
Ratio of effective to actual cross-sectional area	0.01 to 1.00

From the program the output data are $T_p(R,Z)$, $T_g(R,Z)$, $Q(R,Z)$, and the net heat contained in the gas and particles throughout the R,Z-plane. The propellant velocity calculated from the weight flow of hydrogen and the dimensions of the reactor is 36.38 feet per second.

DISCUSSION

In discussing the results several trends will first be shown. This will be done by holding all input data constant except the variable under consideration. This variable will assume a variety of values, and the resulting trend will be plotted. After these results are discussed, there will be a series of figures showing lines of equal $T_p - T_g$ which exist in the reactor model. From these figures an overall picture is shown of the temperature difference between the particles and the gas throughout the reactor cavity. This is done for several sets of different input data, and the resulting change in the equal $T_p - T_g$ lines is shown. In addition to plotting lines of equal $T_p - T_g$, radial plots of $T_p - T_g$ are made at several locations downstream of the inlet of the reactor. These radial plots illustrate the variation of $T_p - T_g$ from the core surface out to the reactor wall.

In figures 4 to 6 the $T_p - T_g$ was obtained from the particles moving next to the surface of the hot gas core. Therefore, these particles receive the maximum amount of heat flux in the reactor model as compared to particles

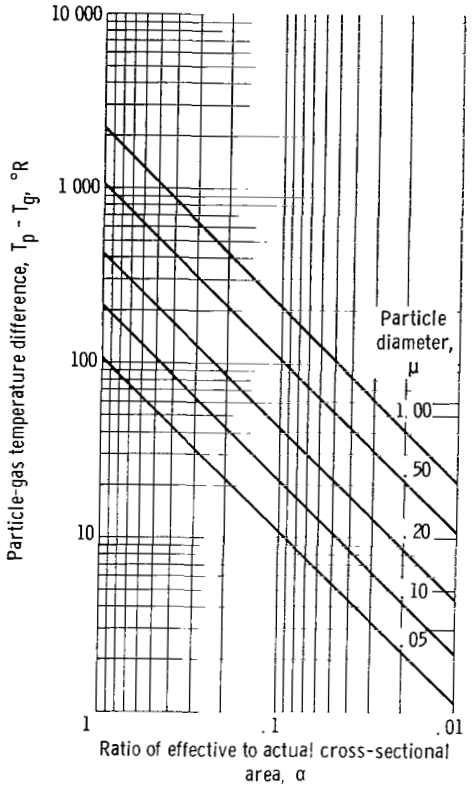

Figure 4. - Comparison of particle-gas temperature difference and ratio of effective to actual cross-sectional area. Core surface temperature, 40 000° R; gas thermal conductivity, 0.852 Btu per foot per hour per °R.

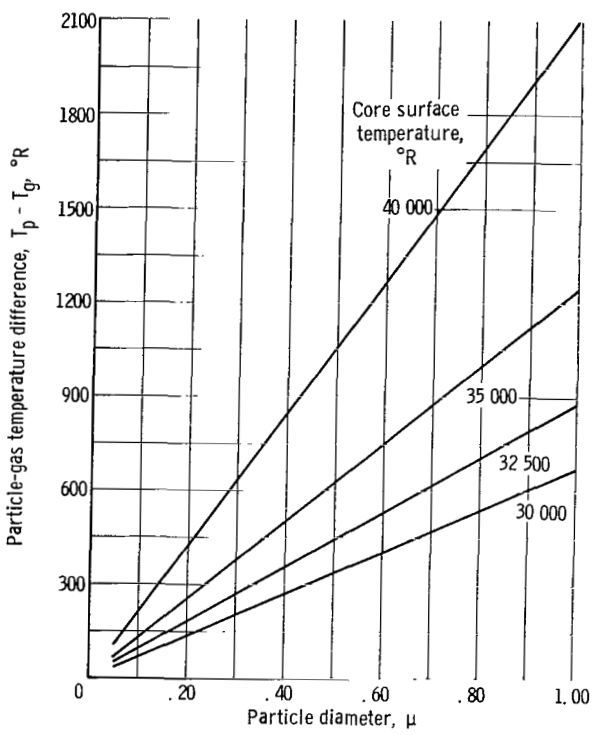

Figure 5. - Comparison of particle-gas temperature difference and particle diameter. Ratio of effective to actual cross-sectional area, 1.0; gas thermal conductivity, 0.852 Btu per foot per hour per °R.

moving in the reactor cavity at greater radial distances. Since $T_p - T_g$ is proportional to the heat flux received, figures 4 to 6 represent maximum cases for extremely high $T_p - T_g$.

The ratio of effective to actual cross-sectional area α is plotted against $T_p - T_g$ in figure 4 for several particle diameters. A significant decrease in $T_p - T_g$ is observed as the value of α decreases from 1.00 to 0.01. A decrease in α corresponding to a decrease in particle diameter was observed in reference 8 for carbon particles. From this observation if a decrease in $T_p - T_g$ due to a smaller particle diameter occurs, then there will be an additional lowering in $T_p - T_g$ due to the decrease in α corresponding to the smaller particle diameter. For figure 4 the gas thermal conductivity is 0.852 Btu per foot per hour per $^{\circ}R$, and the core surface temperature is 40 000° R.

In figure 5 the variation of $T_p - T_g$ with particle diameter is shown for several core surface blackbody temperatures. The ratio of effective to actual cross-sectional area α and the gas thermal conductivity are kept constant at 1.00 and 0.852 Btu per hour per foot per $^{\circ}R$, respectively.

Figure 6 shows the variation of $T_p - T_g$ with core surface blackbody tem-

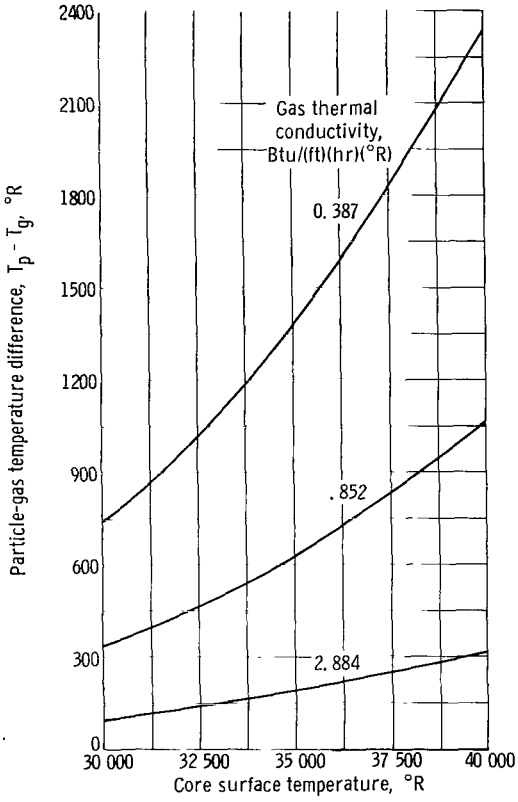

Figure 6. - Comparison of particle-gas temperature difference and core surface temperature. Particle diameter, 0.5 micron; ratio of effective to actual cross-sectional area, 1.0.

perature for several gas thermal conductivities. The range of gas thermal conductivities corresponds to the maximum temperature range hydrogen experiences in this reactor concept. An increase in gas thermal conductivity corresponds to an increase in hydrogen temperature; therefore, the trend is to lower $T_p - T_g$ as the temperature of the hydrogen increases. For figure 6 the particle diameter is kept at 0.50 micron, and the ratio of effective to actual cross-sectional area α is kept at 1.00.

Figure 7 presents plots of equal $T_p - T_g$ in the cavity of a gas-core nuclear rocket model for three sets of conditions. Several trends are shown in this figure. First, as the seed diameter increases from 0.2 to 1.0 micron (figs. 7(a) and (b)), $T_p - T_g$ increases markedly near the surface of the core. However, $T_p - T_g$ still decreases rapidly toward the cavity wall. When the core surface blackbody temperature is increased to 40 000° R (fig. 7(c)), a continued increase in $T_p - T_g$ is shown. At the surface of the core $T_p - T_g$ is very high, but again it decreases quite rapidly away from the core surface. Also shown in figure 7 is the rate at which the particles reach their vaporization temperature. As the particle diameter increases from 0.2 to 1.0 micron (figs. 7(a) and (b)), more than four times the distance or time is required to reach the vaporization temperature. However, when the core surface temperature is raised to 40 000° R (fig. 7(c)), the distance required to vaporize 1.0-micron particles is just slightly longer than that required for a core surface temperature of 32 500° R and particles 0.2 micron in diameter. In figure 7 the reason the lines of equal $T_p - T_g$ slope away from the core surface is that, after the particles start vaporizing at the core, the heat flux increases for any radial position as one moves in the Z-direction. This is due to the fact that the vaporized particles are assumed to be transparent.

In figure 8, radial plots of $T_p - T_g$ are given for several axial locations in the reactor. In this figure the rapid decrease in $T_p - T_g$ is clearly seen as one moves outward from the core surface to the reactor cavity wall. Because of the extremely rapid decrease in $T_p - T_g$ with increasing radial position, only a small percentage of hydrogen gas experiences any severe temperature lag behind the particles.

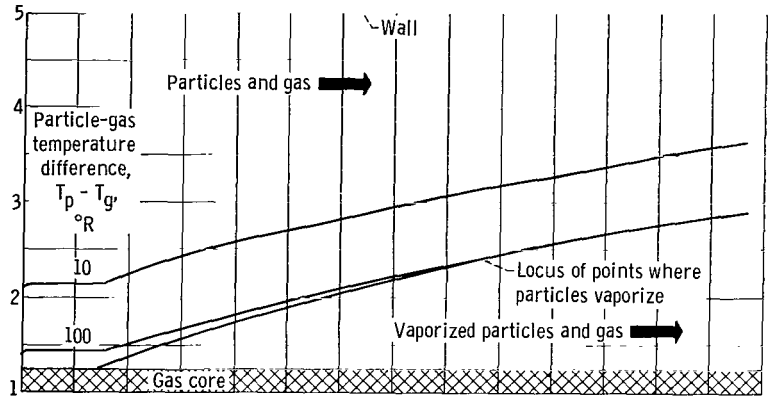

(a) Particle diameter, 0.2 micron; core surface temperature, 32 500° R.

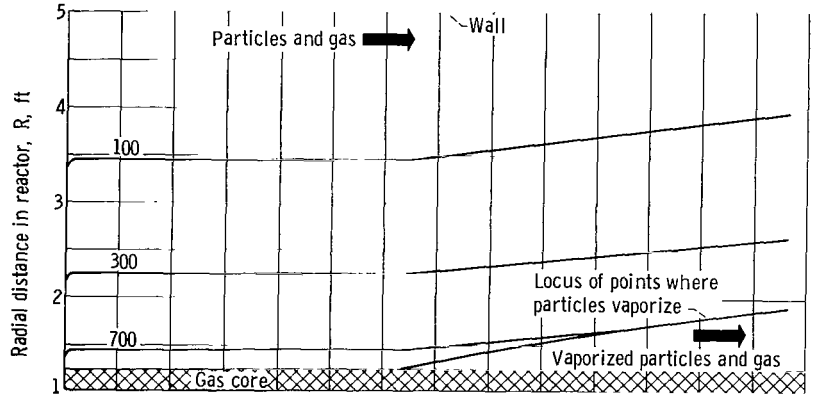

(b) Particle diameter, 1.0 micron; core surface temperature, 32 500° R.

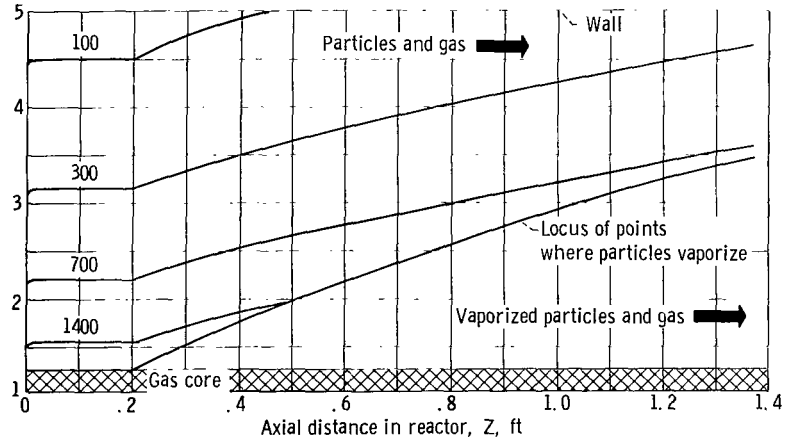

(c) Particle diameter, 1.0 micron; core surface temperature, 40 000° R.

Figure 7. - Particle-gas temperature difference in gas-core reactor. Gas thermal conductivity, 0.852 Btu per hour per foot per °R; ratio of effective to actual cross-sectional area, 1.00.

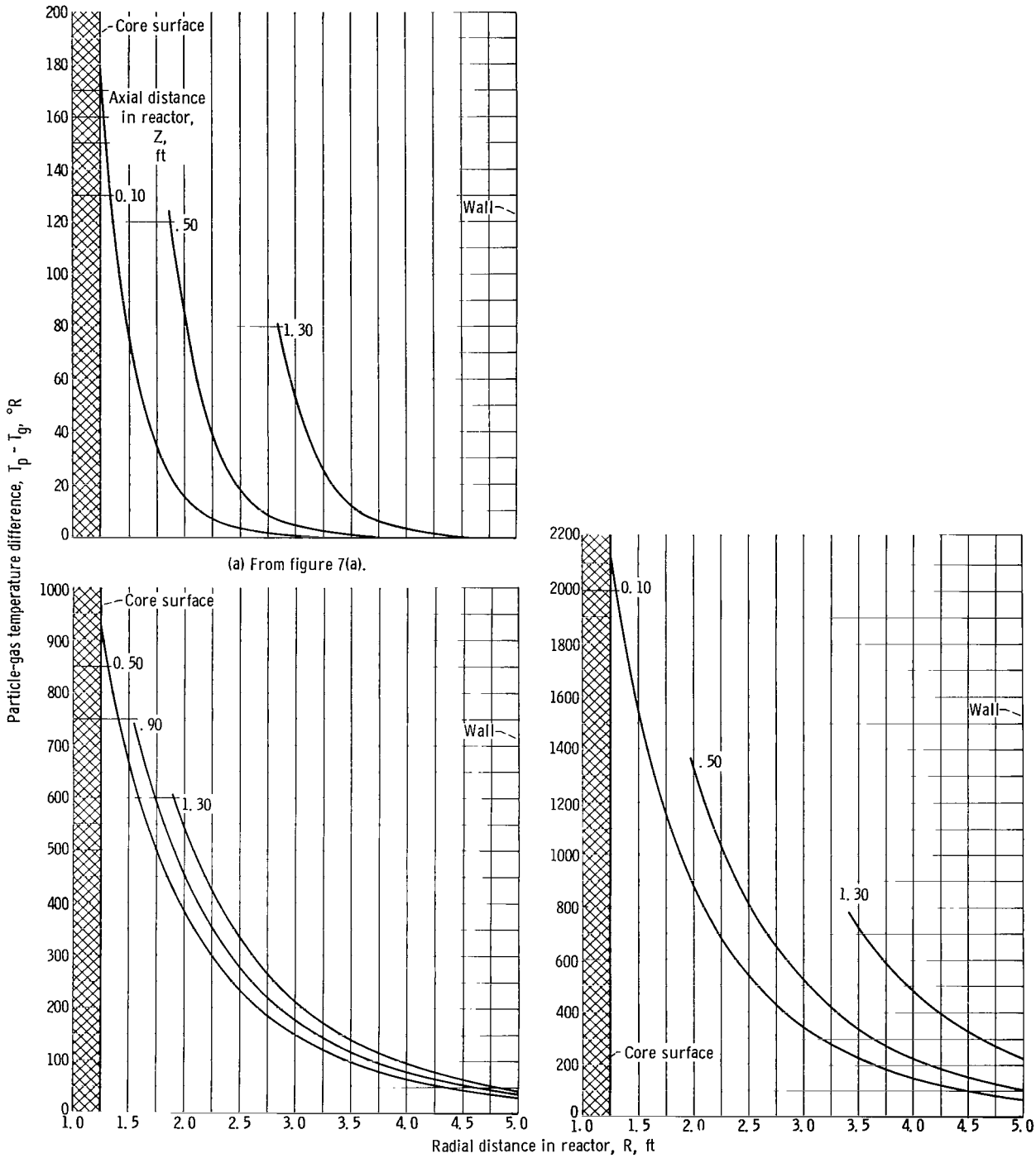

(a) From figure 7(a).

(b) From figure 7(b).

(c) From figure 7(c).

Figure 8. - Radial plots of particle-gas temperature difference.

SUMMARY OF RESULTS

The results of this study indicate some radiative heat transfer characteristics of a flowing gas containing spherical micron size particles. All calculations were carried out by using bulk properties for the gas and particles, constant reactor dimensions, and combinations of the following physical properties: a core surface blackbody temperature of 30 000°, 32 500°, 35 000°, or 40 000°; a particle diameter of 0.05, 0.10, 0.20, 0.50, or 1.00 micron; a gas thermal conductivity of 0.387, 0.852, or 2.884 Btu per foot per hour per °R; and a ratio of effective to actual cross-sectional area of 1.00, 0.10, or 0.01. For these ranges of conditions the following trends were obtained:

1. As the heat flux from the core increased there was a linear increase in the difference between particle temperature T_p and gas temperature T_g when all other properties were assumed constant. In the case of 0.20-micron-diameter particles, a gas thermal conductivity of 0.852 Btu per foot per hour per °R, and a ratio of effective to actual cross-sectional area of 1.00, the $T_p - T_g$ at the core surface increased from 133° to 423° R for an increase in core surface temperature from 30 000° to 40 000° R.

2. There was a linear increase in $T_p - T_g$ proportional to the increase in particle diameter. When the core surface temperature was 40 000° R, the gas thermal conductivity was 0.852 Btu per foot per hour per °R, and the ratio of effective to actual cross-sectional area was 1.00, the $T_p - T_g$ at the core surface increased from 106° R for 0.05-micron particles to 2112° R for 1.00-micron particles.

3. The value of $T_p - T_g$ was inversely proportional to the gas thermal conductivity. For the case of 0.50-micron particles, a core surface temperature of 32 500° R, and a ratio of effective to actual cross-sectional area of 1.00, the $T_p - T_g$ at the core surface decreased from 1013° to 136° R for a gas thermal conductivities of 0.387 and 2.884 Btu per foot per hour per °R, respectively.

4. The value of $T_p - T_g$ was proportional to the ratio of effective to actual cross-sectional area. For the case where the core surface temperature was 40 000° R, the gas thermal conductivity was 0.852 Btu per foot per hour per °R, and the particle diameter was 0.50 micron, the $T_p - T_g$ at the core surface increased from 10° to 1056° R for ratios of effective to actual cross-sectional area of 0.01 and 1.00, respectively.

5. The particle concentration was not a factor in determining $T_p - T_g$. The particle concentration, however, affected the local values of heat flux at the particle surface.

6. As the distance from the heat flux source increased, the $T_p - T_g$ decreased quickly. In the case of 1.0-micron-diameter particles, a gas thermal conductivity of 0.852 per foot per hour per °R, and a ratio of effective to

actual cross-sectional area of 1.00, $T_p - T_g$ decreased from 921° R at the core surface to 300° R at a distance of 1 foot from the core. At the wall of the reactor, which is 3.75 feet from the core surface, $T_p - T_g$ decreased to 31° R.

In view of the overall effects found in this study, it can be concluded that the difference in temperature between the particle and the gas surrounding the particle is such that the propellant-particle mixture can be treated as a continuous gray gas. In the few extreme cases of high particle-gas temperature difference, a sharp decrease occurred with increasing distance from the heat source.

Lewis Research Center,
National Aeronautics and Space Administration,
Cleveland, Ohio, September 28, 1965.

APPENDIX A

DERIVATION OF PARTICLE TEMPERATURE

In order to obtain the equation for the particle temperature as a function of time, an analysis of the gas-particle model (fig. 2) has to be made. An energy balance over a differential spherical shell of hydrogen gas surrounding the particle is performed. The resulting differential equation to solve is

$$\frac{k_g}{r^2}\frac{\partial}{\partial r}\left(r^2\frac{\partial T}{\partial r}\right) = (\rho c_p)_g\frac{\partial T}{\partial \theta} \qquad l > r > a \qquad \text{(A1)}$$

With the two boundary conditions

$$\alpha Q = -4k_g\frac{\partial T}{\partial r} + \frac{4a(\rho c_p)_p}{3}\frac{\partial T}{\partial \theta} \qquad \text{at} \quad r = a \qquad \text{(A2)}$$

$$\frac{\partial T}{\partial r} = 0 \qquad \text{at} \quad r = l \qquad \text{(A3)}$$

the initial condition is

$$T = T_0 \qquad \text{at} \quad \theta = 0 \qquad \text{(A4)}$$

The mean distance between particle centers l can be expressed in the following manner:

$$l^3 = \frac{3}{4\pi N} \qquad \text{(A5)}$$

The following dimensionless variables are introduced:

$$X = \frac{r}{a} \qquad \text{(A6)}$$

$$L = \frac{l}{a} \qquad \text{(A7)}$$

$$U = \frac{X\,(T - T_0)}{T_0} \qquad \text{(A8)}$$

and

$$t = \frac{k_g\theta}{(\rho c_p)_g a^2} \qquad \text{(A9)}$$

Rewriting equation (A1) by introducing equation (A6) yields

$$\frac{k_g}{(\rho c_p)_g} \frac{1}{X^2 a^2} \frac{\partial}{\partial X} \left(X^2 \frac{\partial T}{\partial X} \right) = \frac{\partial T}{\partial \theta} \tag{A10}$$

Equation (A8) can be rewritten

$$T = \frac{UT_0}{X} + T_0 \tag{A11}$$

Taking a derivative with respect to X gives

$$\frac{\partial T}{\partial X} = - \frac{UT_0}{X^2} + \frac{T_0}{X} \frac{\partial U}{\partial X} \tag{A12}$$

Multiplying each side of equation (A12) by $X^2 a$ gives

$$X^2 a \frac{\partial T}{\partial X} = - UT_0 a + T_0 aX \frac{\partial U}{\partial X} \tag{A13}$$

The derivative of equation (A13) with respect to X is

$$\frac{\partial}{\partial X} \left(X^2 a \frac{\partial T}{\partial X} \right) = - T_0 a \frac{\partial U}{\partial X} + T_0 ax \frac{\partial^2 U}{\partial X^2} + T_0 a \frac{\partial U}{\partial X} \tag{A14}$$

or

$$\frac{\partial}{\partial X} \left(X^2 a \frac{\partial T}{\partial X} \right) = T_0 aX \frac{\partial^2 U}{\partial X^2} \tag{A15}$$

Introducing equation (A15) into equation (A10) results in

$$\frac{k_g}{(\rho c_p)_g} \frac{1}{X^2 a^2} \left(T_0 X \frac{\partial^2 U}{\partial X^2} \right) = \frac{\partial T}{\partial \theta} \tag{A16}$$

The derivative of equation (A9) is

$$dt = \frac{k_g}{(\rho c_p)_g a^2} d\theta \tag{A17}$$

The derivative of equation (A8), with X constant, is

$$\partial T = \partial U \frac{T_0}{X} \tag{A18}$$

Combining equations (A17) and (A18) into equation (A16) yields

$$\frac{\partial^2 U}{\partial X^2} = \frac{\partial U}{\partial t} \tag{A19}$$

The Laplace transform of equation (A19), with the initial condition

$$U(X,0) = 0 \tag{A20}$$

is

$$\frac{\partial^2 u(X,S)}{\partial X^2} = Su(X,S) \tag{A21}$$

The solution to equation (A21) is

$$u = A \exp(\sqrt{S}\, X) + B \exp(-\sqrt{S}\, X) \tag{A22}$$

An additional change of variables is made:

$$v = \mathcal{L}\left(\frac{T-T_0}{T_0}\right) = \frac{1}{X}\,\mathcal{L}(U) = \frac{1}{X}\left[A \exp(\sqrt{S}\, X) + B \exp(-\sqrt{S}\, X)\right] \tag{A23}$$

The second boundary condition equation (A3) can be expressed in terms of the new variables as

$$\frac{T_0}{Xa}\frac{\partial U}{\partial X} - \frac{T_0 U}{X^2 a} = 0 \tag{A24}$$

and the Laplace transformation is then

$$\frac{1}{X^2 a}\frac{\partial v(L,S)}{\partial X} = 0$$

or

$$\frac{\partial v(L,S)}{\partial X} = 0 \tag{A25}$$

Expressing the first boundary condition equation (A2) in terms of the new variables by using equations (A17) and (A18) and the derivative of equations (A8) and (A6), which is

$$\partial r = a\partial X \tag{A26}$$

results in

$$\alpha Q = -4k_g \frac{T_0}{aX}\frac{\partial U}{\partial X} + \frac{4a(\rho c_p)_p}{3}\frac{k_g T_0}{X(\rho c_p)_g a^2}\frac{\partial U}{\partial t} + 4k_g \frac{T_0 U}{aX^2} \qquad \text{at } X = 1 \tag{A27}$$

The Laplace transformation gives

$$\frac{\alpha Q}{ST_0} = -\frac{4k_g}{a}\frac{\partial v(1,S)}{\partial X} + \frac{4a(\rho c_p)_p k_g}{3(\rho c_p)_g a^2} Sv(1,S) \tag{A28}$$

Let

$$\varphi = \frac{(\rho c_p)_p}{3(\rho c_p)_g} \tag{A29}$$

Then

$$\frac{\alpha Q a}{k_g S T_0} + \frac{4\partial v(1,S)}{\partial X} = 4\varphi S v(1,S) \tag{A30}$$

When equations (A25) and (A30) are used to eliminate A and B from equation (A23), the result is

$$v(X,S) = \frac{\alpha Q a}{4Xk_g T_0 S}\left\{\frac{\exp\left(-\sqrt{S}\,X\right) - \left(\frac{1 - L\sqrt{S}}{1 + L\sqrt{S}}\right)\exp\left[\sqrt{S}\,(2L - X)\right]}{(1 - \sqrt{S} + \varphi S)\exp(\sqrt{S}) - (1 + \sqrt{S} + \varphi S)\left(\frac{1 - L\sqrt{S}}{1 + L\sqrt{S}}\right)\exp\left[\sqrt{S}(2L - 1)\right]}\right\} \tag{A31}$$

For the particle X = 1,

$$v(1,S) = \frac{\alpha Q a}{4k_g T_0 S}\left(\frac{1}{1 - \sqrt{S}\left\{\frac{\exp\left(\sqrt{S}\right) + \left(\frac{1 - L\sqrt{S}}{1 + L\sqrt{S}}\right)\exp\left[\sqrt{S}\,(2L - 1)\right]}{\exp\left(\sqrt{S}\right) - \left(\frac{1 - L\sqrt{S}}{1 + L\sqrt{S}}\right)\exp\left[\sqrt{S}\,(2L - 1)\right]}\right\} + \varphi S}\right) \tag{A32}$$

For $L \gg 1$ equation (A32) can be approximated by

$$v(1,S) = \frac{\alpha Q a}{4k_g T_0 S}\left(\frac{1}{1 + \sqrt{S} + \varphi S} + \frac{3}{L^3 S}\right) \tag{A33}$$

For the cases used in this study L is approximately 100. Also since $\sqrt{S}$ is much smaller than $1 + \sqrt{S} + \varphi S$ for all S, $\sqrt{S}$ can be dropped from equation (A33):

$$v(1,S) = \frac{\alpha Qa}{4k_g T_0 S}\left(\frac{1}{1+\varphi S} + \frac{3}{L^3 S}\right) \tag{A34}$$

The inverse Laplace transformation of equation (A34) gives

$$T_p - T_0 = \frac{\alpha Qa}{4k_g}\left\{1 - \exp\left[-\frac{3k_g\theta}{a^2(\rho c_p)_p}\right] + \frac{4\pi aNk_g\theta}{(\rho c_p)_g}\right\} \tag{A35}$$

APPENDIX B

DERIVATION OF DIFFERENCE BETWEEN PARTICLE TEMPERATURE AND BULK GAS TEMPERATURE

From an energy balance on the gas-particle model (fig. 2), there is obtained the difference between the particle temperature and the bulk gas temperature. The heat contained in the gas is

$$q_g = \pi a^2 \alpha Q \theta - \frac{4}{3} \pi a^3 (\rho c_p)_p \frac{\alpha Q a}{4 k_g} \left\{ 1 - \exp \left[- \frac{3 k_g \theta}{a^2 (\rho c_p)_p} \right] + \frac{4 \pi a N k_g \theta}{(\rho c_p)_g} \right\} \tag{B1}$$

which can be written as

$$q_g = \frac{4}{3} \pi (l^3 - a^3)(\rho c_p)_g (T_g - T_0) \tag{B2}$$

or as

$$T_g - T_0 = \frac{q_g}{\frac{4}{3} \pi (l^3 - a^3)(\rho c_p)_g} \tag{B3}$$

When equation (B3) is subtracted from equation (A35) and equation (B1) is introduced, the result is

$$T_p - T_g = \frac{\alpha Q a}{4 k_g} \left\{ 1 - \exp \left[- \frac{3 k_g \theta}{a^2 (\rho c_p)_p} \right] + \frac{4 \pi a N k_g \theta}{(\rho c_p)_g} \right\} - \frac{\pi a^2 \alpha Q \theta}{\frac{4}{3} \pi (l^3 - a^3)(\rho c_p)_g} + \frac{a^3 (\rho c_p)_p}{(l^3 - a^3)(\rho c_p)_g} \frac{\alpha Q a}{4 k_g} \left\{ 1 - \exp \left[- \frac{3 k_g \theta}{a^2 (\rho c_p)_p} \right] + \frac{4 \pi a N k_g \theta}{(\rho c_p)_g} \right\} \tag{B4}$$

which can be simplified to

$$T_p - T_g = \left(1 + \frac{a^3 (\rho c_p)_p}{(l^3 - a^3)(\rho c_p)_g} \right) \left(\frac{\alpha Q a}{4 k_g} \left\{ 1 - \exp \left[- \frac{3 k_g \theta}{a^2 (\rho c_p)_p} \right] + \frac{4 \pi a N k_g \theta}{(\rho c_p)_g} \right\} \right) - \frac{3 a^2 \alpha Q \theta}{4 (l^3 - a^3)(\rho c_p)_g} \tag{B5}$$

Since $l^3 \ggg a^3$

$$T_p - T_g = \frac{\alpha Q a}{4k_g} \left\{ 1 - \exp \left[- \frac{3k_g \theta}{a^2 (\rho c_p)_p} \right] + \frac{4\pi a N k_g \theta}{(\rho c_p)_g} \right\} - \frac{a^2 \alpha Q \theta}{\frac{4(\rho c_p)_g}{3} \frac{3}{4\pi N}} \qquad \text{(B6)}$$

This reduces to

$$T_p - T_g = \frac{\alpha Q a}{4k_g} \left\{ 1 - \exp \left[- \frac{3k_g \theta}{a^2 (\rho c_p)_p} \right] \right\} \qquad \text{(B7)}$$

REFERENCES

1. Rom, Frank E.; and Ragsdale, Robert G.: Advanced Concepts for Nuclear Rocket Propulsion. Proceedings of the NASA - University Conference on the Science and Technology of Space Exploration, vol. 2, NASA SP-11, 1962, pp. 62-75. (Also available as NASA SP-20.)

2. Weinstein, Herbert; and Ragsdale, Robert G.: A Coaxial Flow Reactor - A Gaseous Nuclear-Rocket Concept. Reprint No. 1518-60, ARS, 1960.

3. Ragsdale, Robert G.; and Einstein, Thomas H.: Two-Dimensional Gray-Gas Radiant Heat Transfer in a Coaxial-Flow Gaseous Reactor. NASA TN D-2124, 1964.

4. Krascella, N. L.: Theoretical Investigation of the Absorption and Scattering Characteristics of Small Particles. NASA CR-210, 1965.

5. Stull, V. R.; and Plass, G. N.: Emissivity of Dispersed Carbon Particles. J. Opt. Soc. Am., vol. 50, no. 2, Feb. 1960, pp. 121-129.

6. Marteney, P. J.: Experimental Investigation of the Opacity of Small Particles. NASA CR-211, 1965.

7. Johnstone, H. F.; Pigford, R. L.; and Chapin, J. H.: Heat Transfer to Clouds of Falling Particles. A. I. Ch. E. Trans., vol. 37, 1941, pp. 95-133.

8. Lanzo, Chester D.; and Ragsdale, Robert G.: Experimental Determination of Spectral and Total Transmissivities of Clouds of Small Particles. NASA TN D-1405, 1962.

9. Lanzo, Chester D.; and Ragsdale, Robert G.: Heat Transfer to a Seeded Flowing Gas from an Arc Enclosed by a Quartz Tube. Paper Presented at Heat Transfer and Fluid Mech. Inst. Meeting, Berkeley (Calif.), June 10-12, 1964.

10. Carslaw, H. S., and Jaeger, J. C.: Conduction of Heat in Solids. Second ed., Oxford Univ. Press, 1959.

11. Sleicher, Charles A., Jr.; and Churchill, Stuart W.: Radiant Heating of Dispersed Particles. Industrial and Engineering Chemistry, vol. 48, no. 10, Oct. 1956, pp. 1819-1824.

12. McAlister, A.; Keng, Edward; and Orr, Clyde, Jr.: Heat Transfer to a Gas Containing a Cloud of Particles. Georgia Inst. Tech., June 1965.

13. McAdams, William H.: Heat Transmission. Third ed., McGraw-Hill Book Co., Inc., 1954.

14. Grier, Norman T.: Calculation of Transport Properties and Heat-Transfer Parameters of Dissociated Hydrogen. NASA TN D-1406, 1962.

"The aeronautical and space activities of the United States shall be conducted so as to contribute . . . to the expansion of human knowledge of phenomena in the atmosphere and space. The Administration shall provide for the widest practicable and appropriate dissemination of information concerning its activities and the results thereof."

—NATIONAL AERONAUTICS AND SPACE ACT OF 1958

NASA SCIENTIFIC AND TECHNICAL PUBLICATIONS

TECHNICAL REPORTS: Scientific and technical information considered important, complete, and a lasting contribution to existing knowledge.

TECHNICAL NOTES: Information less broad in scope but nevertheless of importance as a contribution to existing knowledge.

TECHNICAL MEMORANDUMS: Information receiving limited distribution because of preliminary data, security classification, or other reasons.

CONTRACTOR REPORTS: Technical information generated in connection with a NASA contract or grant and released under NASA auspices.

TECHNICAL TRANSLATIONS: Information published in a foreign language considered to merit NASA distribution in English.

TECHNICAL REPRINTS: Information derived from NASA activities and initially published in the form of journal articles.

SPECIAL PUBLICATIONS: Information derived from or of value to NASA activities but not necessarily reporting the results of individual NASA-programmed scientific efforts. Publications include conference proceedings, monographs, data compilations, handbooks, sourcebooks, and special bibliographies.

Details on the availability of these publications may be obtained from:

SCIENTIFIC AND TECHNICAL INFORMATION DIVISION

NATIONAL AERONAUTICS AND SPACE ADMINISTRATION

Washington, D.C. 20546